Membrane interaction of off-pathway prion oligomers and lipid-induced on-pathway intermediates during prion conversion: A clue for neurotoxicity

Sophie Combet, Fabrice Cousin, Human Rezaei, Sylvie Noinville

Elsevier Editorial System(tm) for BBA - Biomembranes

Manuscript Draft

Manuscript Number:

Title: Membrane interaction of off-pathway prion oligomers and lipid-induced on-pathway intermediates during prion conversion: a clue for neurotoxicity.

Article Type: Regular Paper

Keywords: Prion protein; lipid membrane; oligomer; leakage; conformational change

Corresponding Author: Dr. Sylvie Noinville, Ph.D.

Corresponding Author's Institution: CNRS-Sorbonne Université

First Author: Sophie Combet, PhD

Order of Authors: Sophie Combet, PhD; Fabrice Cousin, PhD; Human Rezaei, PhD; Sylvie Noinville, Ph.D.

Abstract: Soluble oligomers of prion proteins (PrP), produced during amyloid aggregation, have emerged as the primary neurotoxic species, instead of the fibrillar end-products, in transmissible spongiform encephalopathies. However, whether the membrane is among their direct targets, that mediate the downstream adverse effects, remains a question of debate. Recently, questions arise from the formation of membrane-active oligomeric species generated during the □-aggregation pathway, either in solution, or in lipid environment. In the present study, we characterized membrane interaction of off-pathway oligomers from recombinant prion protein generated along the amyloid aggregation and compared to lipid-induced intermediates produced during lipid-accelerated fibrillation. Using calcein-leakage assay, we show that the soluble prion oligomers are the most potent in producing leakage with negatively charged vesicles. Binding affinities, conformational states, mode of action of the different PrP assemblies were determined by thioflavin T binding-static light scattering experiments on DOPC/DOPS vesicles, as well as by FTIR-ATR spectroscopy and specular neutron reflectivity onto the corresponding supported lipid bilayers. Our results indicate that the off-pathway PrP oligomers interact with lipid membrane via a distinct mechanism, compared to the inserted lipid-induced intermediates. Thus, separate neurotoxic mechanisms could exist following the puzzling intermediates generated in the different cell compartments. These results not only reveal an important regulation of lipid membrane on PrP behavior but may also provide clues for designing stage-specific and prion-targeted therapy.

Suggested Reviewers: Vincent Raussens
Structure and Function of Biological Membranes Laboratory, Université Libre de Bruxelles
Vincent.Raussens@ulb.ac.be
expert in amyloid/membrane interaction, in infrared spectroscopy

Mireille MAE Claessens

Department of Nano-BioPhysics, University of Twente
m.m.a.e.claessens@utwente.nl
expert in amyloid/lipid interaction, biophysics

Alexandros Koutsioumpas
Jülich Centre for Neutron Science, Heinz Maier-Leibnitz Zentrum (MLZ)
a.koutsioumpas@fz-juelich.de
expert in neutron scattering and supported lipid bilayers

Sheena Radford
School of Biochemistry and Molecular Biology, University of Leeds
s.e.radford@leeds.ac.uk
expert in biophysics, in amyloids and protein aggregation

Dear Pr Hans Vogel, Executive Editor,

I would like to request you to consider the attached manuscript entitled *Membrane interaction of off-pathway prion oligomers and lipid-induced on-pathway intermediates during prion conversion: a clue for neurotoxicity* by Sophie Combet, Fabrice Cousin, Human Rezaei, Sylvie Noinville for publication in ***BBA-biomembranes*** as an original article. The script has been prepared in accordance with the *Guide to Authors* and has not been submitted for publication elsewhere.

I believe that the findings of this study are relevant to the scope of the journal and will be of great interest to its readership considering the very recent special issue of BBA-biomembranes devoted to protein aggregation and misfolding at the cell membrane interface. While many studies have investigated the ability of amyloid aggregates to bind the cell membrane and induce disruption of lipid bilayer structure correlating with their cytotoxicities, I have not come across a paper that compares the membrane interaction of lipid-mediated amyloid aggregates and off-pathway oligomers produced along amyloid fibrillation to track the putative key oligomeric toxic species. We conducted different biophysical experiments such as detailed FTIR, neutron reflectometry, dye-leakage and dye-binding assays, static and dynamic light scattering to characterize the effect of SEC-purified oligomers of prion protein generated along the aggregation pathway onto well-characterized model lipid membrane. We laid emphasis on the role of these discrete off-pathway oligomers compared to the on-going lipid-induced intermediates of prion protein, shading light on the very intricate problem of the fate of the different amyloid assemblies generated *in vivo* at lipid interface. I feel that our paper by proposing distinct interactions with lipid membrane of the soluble discrete oligomers compared to the membrane-induced intermediates might point the occurrence of different mechanism of cytotoxicities during neurodegeneration.

All the authors have read the manuscript and agree on its contents, and we have followed all required ethical guidelines. There are no conflicts of interest to declare.

I look forward to hearing from you.

Yours sincerely,

Dr Sylvie Noinville

Membrane interaction of off-pathway prion oligomers and lipid-induced on-pathway intermediates during prion conversion: a clue for neurotoxicity.

Sophie Combet[a], Fabrice Cousin[a], Human Rezaei[b], and Sylvie Noinville[c,*]

[a]Laboratoire Léon-Brillouin, UMR 12 CEA-CNRS, Université Paris-Saclay, CEA-Saclay, F-91191 Gif-sur-Yvette CEDEX, France.

[b]Laboratoire de Virologie et Immunologie Moléculaires, UR892, Institut National de la Recherche Agronomique (INRA), F-78352 Jouy-en-Josas, France.

[c]Laboratoire MONARIS, UMR 8233, Sorbonne Université, CNRS, F-75005 Paris, France.

ABSTRACT

Soluble oligomers of prion proteins (PrP), produced during amyloid aggregation, have emerged as the primary neurotoxic species, instead of the fibrillar end-products, in transmissible spongiform encephalopathies. However, whether the membrane is among their direct targets, that mediate the downstream adverse effects, remains a question of debate. Recently, questions arise from the formation of membrane-active oligomeric species generated during the β-aggregation pathway, either in solution, or in lipid environment. In the present study, we characterized membrane interaction of off-pathway oligomers from recombinant prion protein generated along the amyloid aggregation and compared to lipid-induced intermediates produced during lipid-accelerated fibrillation. Using calcein-leakage assay, we show that the soluble prion oligomers are the most potent in producing leakage with negatively charged vesicles. Binding affinities, conformational states, mode of action of the different PrP assemblies were determined by thioflavin T binding-static light scattering experiments on DOPC/DOPS vesicles, as well as by FTIR-ATR spectroscopy and specular neutron reflectivity onto the corresponding supported lipid bilayers. Our results indicate that the off-pathway PrP oligomers interact with lipid membrane *via* a distinct mechanism, compared to the inserted lipid-induced intermediates. Thus, separate neurotoxic mechanisms could exist following the puzzling intermediates generated in the different cell compartments. These results not only reveal an important regulation of lipid membrane on PrP behavior but may also provide clues for designing stage-specific and prion-targeted therapy.

KEYWORDS

Prion protein; lipid membrane; oligomer; leakage; conformational change

1. Introduction

Prion protein (PrP) misfolding is associated with a range of deadly neuropathological diseases, including bovine spongiform encephalopathy in cattle, scrapie in sheep, and Creutzfeld-Jacob in human, characterized by the accumulation of insoluble proteinaceous aggregates inside the infected tissues [1]. The mechanisms that trigger the structural transition from mainly α-helical cellular PrP (PrP^{C}) to its β-sheeted enriched pathological "scrapie" conformer (PrP^{Sc}) are still unclear. PrP/membrane interactions are believed to be essential to the function of PrP in the cell since the protein is localized in close proximity to plasmatic membranes [2-4]. Several converging lines of evidence suggest that this interaction promotes various precursors to aggregation-prone states involved in the amyloid fibrils [5]. As proposed by Collinge *et al.* [6], the prion propagation and toxicity *in vivo* would be kinetically controlled by the interaction of the prion strain type and the host environment. Neurotoxicity would be mediated by lethal PrP species, distinct from the pathological PrP^{Sc} [7]. For example, there is a compelling evidence suggesting that PrP aggregates of low molecular weight or soluble oligomers disrupt membranes and/or induce the formation of ion channels, possibly leading to cellular membrane depolarization [8]. It has been shown that the prion proteins induce ion channel current with defined conductance states in planar lipid bilayers [9]. More recently, neurotoxic mutants of PrP induce spontaneous ionic current in cultured cells [10].

Membrane surface, depending on its chemical composition, is known to act as a catalytic site that promotes the misfolding and aggregation of bound amyloidogenic proteins [11, 12]. Recombinant PrP in monomeric forms has been shown to bind lipids and this binding involves the unfolding of helical structures present in the C-terminal globular part [13-16], while recombinant PrP in β-structure using reducing conditions was found to form amyloid fibers when interacting with lipid membrane [17]. *In vitro* experiments show that negatively

charged lipids accelerate PrP fibrillation [18, 19]. Most notably, aggregated recombinant PrP in the presence of anionic lipids, such as phosphatidylglycerol, leads to the formation of insoluble particles showing infectivity, supporting a crucial role for lipid-PrP interaction into PrP conversion [20]. Moreover, the highly conserved middle region of PrP, spanning the residues 105-135 consisting of a positively charged region and a hydrophobic domain, is essential for lipid-induced PrP conversion. Disease-associated mutants, encompassing mutation in this middle region, have distinct lipid interaction compared to the wild type PrP, suggesting the relevance of PrP-lipid interaction in forming intermediates linked to pathogenic changes [21]. Like many other amyloidogenic proteins, PrP oligomeric assemblies could disrupt membrane structural integrity, which is a first indicator of toxic function [22, 23]. However, the difficulties remain to assess the role of each intermediate on the β-aggregation pathway from the different recombinant constructs produced *in vitro* to elucidate the neurotoxicity mechanism of oligomeric intermediates generated *in vivo* [24]. Regarding the complexity of this issue, the necessity of simplifying the membrane interaction with disruptive species produced along the pathway of *in vitro* β-aggregation in solution is evident. Since the lipid membrane could act as a template for β-aggregation of amyloidogenic proteins, deciphering the mode of action of oligomers produced in solution from those, if any, produced during interaction with lipid membrane is more and more necessary. Furthermore, the question concerning the mode of action, as well as the variation of the permeabilization mechanism depending on the amyloid oligomeric states and its link with their structural identity, remains fully open.

In a previous work, we demonstrated the sequential formation of structurally distinct soluble PrP oligomers, either off-pathway, or on-pathway, corresponding to 12-mers or 36-mers respectively, as depicted in Scheme 1 [25]. The soluble oligomers of higher molecular weight, corresponding to 36-mers of PrP as characterized by SAXS, are able to form fibrils, whereas

the soluble 12-mers remain in equilibrium with the monomeric forms [26, 27]. We also showed that the well-characterized highly homogeneous populations of both off- and on-pathway PrP oligomers are stable at physiological pH, and that the discrete 12-mers could disrupt negatively charged membrane containing phosphatidylinositol lipid [18].

Scheme 1. Schematic representation of *in vitro* polymerization of PrP in solution leading to the formation of soluble oligomers, either on-, or off-pathway. Only the off-pathway oligomers are not converted into prion fibrils.

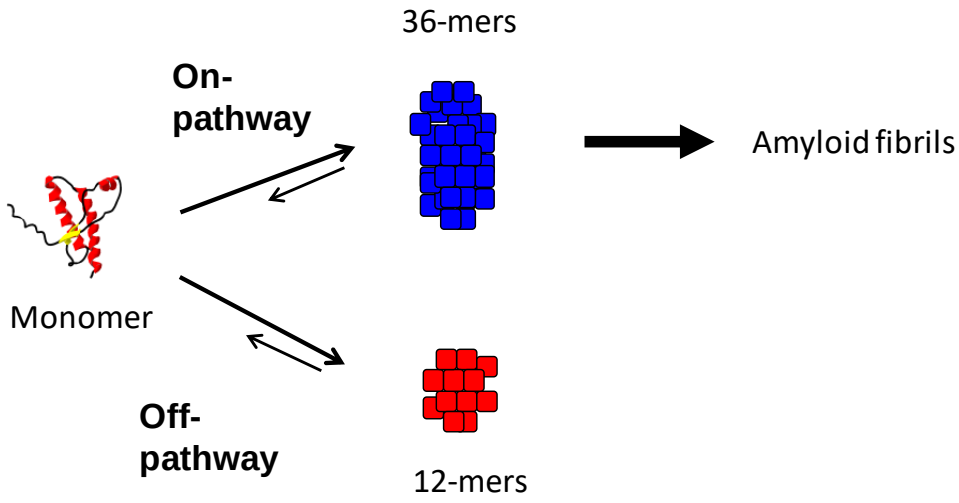

In the present study, our goal was to detail the interaction of the off-pathway 12-mers produced in solution along PrP β-aggregation compared to the on-going lipid-induced PrP intermediates generated at the early stage of the amyloid fibrillation with model membranes. To decipher the role of soluble intermediates, the propensities of lipid membrane disruption by off-pathway oligomers have been checked by calcein-leakage assays on DOPC/DOPS vesicles and compared to on-pathway PrP assemblies. ThT is the most widely used amyloid marker for both *in vitro* and *in vivo* amyloid fibrillation characterization [28]. ThT binding assays combined to SLS measurements enable to follow the lipid-induced fibrillation of PrP monomer at the surface of lipid vesicles, and to detect ThT positive

intermediates during interaction of the off-pathway oligomers with the lipid membrane. The interactions of the soluble oligomers with membrane were also studied by FTIR-ATR and specular neutron reflectometry (SNR) experiments and compared to the lipid-induced PrP intermediates. For both ATR and SNR techniques, the model lipid bilayer was obtained by the fusion of DOPC/DOPS vesicles to obtain well-characterized supported lipid bilayers (SLBs) [29], as well as relevant biomimetic lipid composition for mammalian neurons [30]. The conformational states of lipid-bound intermediates along *in situ* lipid-induced PrP conversion were determined by spectral analysis of Amide I' band. A "snapshot" of the lipid-bound intermediates was taken at the early stage of lipid-induced PrP conversion and characterized by SNR experiments at identical protein to lipid ratio used for ATR. SNR enables to observe the Å-level resolution changes in the thickness and density of lipid bilayers as a result of protein binding, by determining the in-plane averaged scattering length density (SLD) profile normal to the surface [31, 32]. Recently, SNR was used to examine in details the membrane interaction of amyloidogenic proteins to provide insight into the mechanism of amyloid toxicity [33-35].

Based on the functional and structural data recorded by *in vitro* fluorescence assays and biophysical techniques, such as SNR and FTIT-ATR, the present study aims at tracking the putative membrane-active β-structured oligomers along the amyloid β-aggregation in solution from those induced *via* confinement of monomers to a lipid membrane.

2. Materials and Methods

2.1 Materials

DOPC (1,2-dioleoyl-*sn*-glycero-3-phosphocholine) and DOPS (1,2-dioleoyl-*sn*-glycero-3-phospho-L-serine) were purchased from Avanti-Polar, Triton-X-100 from Pharmacia biotech, MOPS (4-morpholinepropanesulfonic acid), sodium citrate, triethylammonium acetate,

sodium dodecyl sulphate (SDS) from VWR, D_2O from Eurisotop, calcein , thioflavin T (ThT), and chloride salt from Sigma-Aldrich. Stock (1 mM) solutions of ThT were prepared by dissolving ThT in double-distilled water and its concentration was determined using a molar extinction coefficient of 24,420 M^{-1} cm^{-1} at 420 nm. ThT was stored at 4°C, protected from light.

2.2 Expression of the PrP monomers and purification of the soluble PrP oligomers

N-truncated ovine $PrP^{103-234}$ (ARQ variant) was expressed and purified as described previously [36]. The soluble oligomers were obtained by incubation of the solution of $PrP^{103-234}$ at a concentration of 80 µM in 20 mM citrate buffer, at pH 3.4 and 50°C, for 8 min in a Perkin Elmer GenAmp2400 thermocycler, as described previously [27] (Figure S1 in the Supporting Information). The fraction corresponding to the 12-mer was collected in triethylammonium acetate buffer after separation by size-exclusion chromatography (SEC) using Akta FPLC and lyophilized before use in the appropriate hydrogenated or deuterated buffer. The fraction corresponding to the 36-mer was collected in citrate buffer and then exchanged with MOPS buffer at pH 6 using micro-spin column immediately before calcein leakage assays.

2.3 Preparation of the liposomes for SLBs

Solutions of the DOPC/DOPS mixtures in chloroform were dried under vacuum, until the lipids formed a thin layer inside the flask. The lipid films were then suspended in the desired buffer (10 mM MOPS, 150 mM NaCl, pH 7.4), either in D_2O for ATR, or in H_2O for SNR, experiments at the concentration of 2 mg/mL. The resulting suspension was freeze-thawed three times before extrusion using a Northern lipids apparatus (Vancouver) through two stacked 0.1 µm polycarbonate filters (Millipore) to obtain large unilamellar vesicles (LUV)

with mean hydrodynamic diameters of 110 ± 10 nm, measured by DLS. For the SLBs, the suspension of DOPC/DOPS (molar ratio 7:3) LUVs was extruded on a 0.05 μm polycarbonate filter and was diluted to 0.1 mg/mL lipids in buffer containing 2 mM $CaCl_2$.

2.4 Calcein-entrapped liposome assay

Calcein was dissolved in 10 mM MOPS and 100 mM KCl at pH 7 by repeated vortexing for 30 min at room temperature, to a final concentration of 80 mM. The chloroform solution containing 10 mg of lipid was evaporated under nitrogen and resuspended in calcein solution. The resulting mixture was passed after extrusion through a Sephadex-G25 column (Amersham Biosciences) in the desired buffer, to remove the non-entrapped dye. The suspensions of calcein-entrapped vesicles were monodisperse, and their mean size, as measured by DLS, was 120 ± 15 nm.

An increase in the fluorescence intensity of the dye-entrapped liposomes after incubation with monomer or oligomers of PrP indicated a protein-induced liposomal leakage. The experiments were run at 18°C in a 2 × 10 mm quartz cuvette. Briefly, concentrated protein samples were diluted in a suspension of vesicles in 10 mM MOPS and 100 mM KCl at pH 7, so as to have a final protein concentration ranging from 10 to 500 nM. The medium was stirred continuously to allow a rapid mixing of the protein and vesicles. The samples were excited at 492 nm, and their emission was recorded at 520 nm, using a Jasco FP-777 spectrofluorimeter. The total release of calcein was achieved by the addition of Triton X-100 at a final concentration of 0.05 % (*v*/*v*) at the end of each titration series, so that the maximum fluorescence intensity could be determined. The percentage of leakage was then calculated over the course of the 10 min experiment according to previously described procedures [18]. The experiments were generally repeated at least two times with different, fresh preparations of vesicles. The experimental uncertainty was estimated as ± 5% of the measured value.

2.5 Light-scattering/ThT fluorescence correlation experiments

The static light-scattering (SLS) fluorescence kinetics experiments were performed on a homemade device using a 407 nm laser beam for the excitation of ThT and using three other lasers (473, 533, and 633 nm) for the SLS measurements. Stock solutions of ThT were prepared in 20 mM MOPS buffer to a final concentration of 3 mM. This solution was then filtered on a 0.2 µm pore-sized filter. Liposomes of DOPC/DOPS (molar ratio 7:3) of 110 nm-diameter sized were incubated at 25°C in a 2-mm cuvette in the presence of 100 µM ThT before addition of PrP samples in 20 mM MOPS at pH 7. The emission fluorescence at 485 nm and the light-scattered signals were recorded at a 112° angle. Signal processing was achieved by a homemade Matlab program [26].

2.6 Sample preparation and FTIR spectra acquisition

FTIR-spectra were recorded on a Bruker Equinox spectrometer equipped with a Mercury Cadmium Telluride detector. The resolution was set at 4 cm^{-1}. The spectrometer was continuously purged with dry air. A 45° cut silicon crystal, providing 30 internal reflections at the liquid/crystal interface, was freshly cleaned in a solution of 4:1 (*v*/*v*) concentrated sulfuric acid (H_2SO_4) and 30% hydrogen peroxide (H_2O_2) followed by extensive rinsing with deionized water and drying under nitrogen gas before being mounted in an ATR liquid cell. The ATR cell was filled with the 10 mM MOPS and 150 mM NaCl buffer in D_2O and a reference infrared spectrum was collected. A supported lipid bilayer was formed by the spontaneous adsorption of DOPC/DOPS (molar ratio 7:3) vesicles at 0.1 mg/mL (lipid concentration) onto the freshly-cleaned silicon surface [29]. After 30 minutes of contact, the cell was rinsed with deuterated buffer and the ATR spectrum was acquired to quantify the amount of lipid deposited on the silicon crystal (as calculated using the intensity of the infrared stretching band attributed to the lipid carbonyl at 1730 cm^{-1}). The cell was then filled

with the PrP prepared in deuterated solution at pD 7. Interferograms were recorded as for the reference spectrum and transformed to the ATR corrected absorption spectrum of the adsorbed protein for four hours. Each spectrum was the average of 128 scans. The zero time-point for the adsorption kinetics experiments was set to the start of the contact of the protein solution with the lipid bilayer. The integrated absorbance of the Amide I' band was used to determine the amount of PrP adsorbed onto the SLBs and expressed as Γ in mg/m^2 [37].

2.7 FTIR spectral analysis

The broad Amide I' band in the spectral range of 1600-1700 cm^{-1} is attributed to the carbonyl peptide stretching vibrational modes and it reveals the extent of the secondary structure of the protein. An identical spectral decomposition was found for the analysis of the Amide I' band that was suitable for both the free and lipid-bound PrP species, in such a manner that the extent of the different types of secondary structures could be determined for comparison . The spectral range of conformational interest, *i.e.* the Amide I' band around 1600-1700 cm^{-1}, was analyzed using the curve-fitting procedure as described previously for monomeric PrP and applied to the oligomeric species with the aid of a second derivative analysis [18]. These component bands were assigned according to our previous work and according to the infrared analysis of β-structured or β-aggregated proteins [38-40]. The major peptide carbonyl contributions at 1630 and 1650 cm^{-1} correspond to β-sheets and α-helices in D_2O, respectively. Furthermore, the infrared component band that appears at 1614 cm^{-1} is assigned to the β-structures corresponding to the extended intermolecular β-sheets, and corresponds to the amyloid structures [41]. The component band at 1623 cm^{-1}, that is found in the IR spectra of soluble oligomers in the deuterated buffer, is indicative of β-structure with stronger hydrogen bonds than the component corresponding to a band at 1630 cm^{-1}. This latter band is indeed generally assigned to intramolecular β-sheets in parallel conformation[40].

The least-square iterative curve-fitting program (in Origin software) was used to only adjust the intensity parameter of each component band for each spectrum, while the half bandwidth at half height, and both the band positions and the profile were fixed. The area of each Amide I' component band is expressed as the percentage of the sum of the areas of all of the Amide I' component bands in the spectral range from 1600 to 1700 cm^{-1}. The contents in the different secondary structural elements were given for the pure monomer and the off-pathway oligomers in solution, determined from spectra recorded in transmission and given in Table S1 in the Supporting Information.

2.8 Sample preparation for specular neutron reflectivity

The model membranes, consisting of a single phospholipid bilayer composed of both the zwitterionic DOPC lipid and the negatively charged DOPS lipid (at 7:3 molar ratio), were prepared on a silicon substrate. Round single crystals of silicon of 5.1 cm diameter and 0.5 cm thickness were used and freshly cleaned like for ATR experiments (see above). The silica-coated silicon plates were then mounted in liquid-cells to perform the lipid bilayer deposition by liposome fusion, following the same protocol as described above. Briefly, the solutions of *h*-DOPC/*h*-DOPS (7:3) SUV were injected in the SNR liquid cell at a final lipid concentration of 0.1 mg/mL in MOPS buffer containing 2 mM $CaCl_2$. The lipid bilayer was incubated for 30 min before rinsing with the desired contrast medium, provided by two buffers at pH or pD 7.2 containing 10 mM MOPS, either in 100% D_2O, or in 100% H_2O. The characterization of the SLB was made at the two contrasts before injection of the PrP species at a monomer equivalent concentration of 5 µM. This corresponded to a protein/lipid mol/mol ratio of 6.3:1 and 4.5:1 for the monomers and 12-mers, respectively. The protein layer was characterized after 30 min of adsorption in stationary conditions to ensure identical interaction with the membrane, as described in ATR experiments, and rinsed with the appropriate buffer. The

study at the early stage of formation of the lipid-bound states ensures to characterize oligomeric states by SNR rather than fibrillar end-products.

We verified *in situ* that the SNR curves did not evolve over time by combining several reflectivity spectra over a total duration of 4 hours. Since no changes occurred (the reflectivity curves were superimposed), the spectra were summed. The sample cells were kept at a temperature of 25.0 ± 0.5°C all along the measurements, under the control of a temperature bath, to ensure a fluid state of the membranes.

2.9 Specular neutron reflectivity

The SNR measurements were performed at the Laboratoire Léon-Brillouin (Saclay, France) using the horizontal-sample reflectometer EROS [42]. In a SNR experiment, specular reflection is measured as a function of the wave vector transfer q, perpendicular to the surface, with $q = (4\ \pi\ /\ \lambda)\ \sin\theta$, where θ is the angle and λ is the wavelength of the incident neutron beam. The wavelength of the incident neutrons was between 2 and 20 Å for EROS reflectometer [42]. We used the time-of-flight configuration with the beam pulsed by a double chopper system with variable phase. The contrast variation method was employed by using aqueous buffer solutions of different scattering length densities (SLD), in 100% D_2O or 100% H_2O buffer (with respective SLD of 6.34×10^{-6} and -0.56×10^{-6} Å^{-2}), allowing us to enhance the sensitivity of the measurements. The data were recorded at two fixed incident angles, respectively 1.34° and 2.5° for D_2O and 0.6° and 1.8° for H_2O, in order to cover the desired q-range. The incoming neutron white beam was reflected at the silicon/water interface from the silicon which is almost transparent to neutrons. Data were analyzed using the Motofit software [43]. The experimental resolution of the spectrometer (around 10%) was taken into account in the calculation. In a SNR experiment, the intensity of the curves arose from constructive interferences of the reflected neutron beams from the surface and the interfaces

of the successive layers composing the sample. Each layer is characterized by its SLD, *i.e.* its ability to scatter neutrons, its thickness, and a roughness parameter (*i.e.* the width of the interface between two adjacent layers assuming that the profile between these two adjacent layers can be described by an error function). The SLD of a molecule is directly linked to its chemical composition. For organic compounds, it is mainly sensitive to hydrogen isotopes (H and D) since he coherent length of H is very different to those of other atoms constitutive of organic matter (D, C, O, N) which have coherent lengths of the same order. The SLD of a layer that contains several types of objects is the average of the SLD of the objects weighted by their volume fraction within the layer. This enables to obtain the solvent content of any layer (*i.e.* the volume fraction occupied by the aqueous buffer (prepared in 100% D_2O or H_2O).

Four- or five-layer models (depending on the presence of an extra protein layer or not) were used to fit the reflectivity profiles, a layer being defined as a homogeneous region: (*i*) the silicon oxide (SiO_2), (*ii*) the inner polar head chains, (*iii*) the inner and outer hydrophobic acyl chains, (*iv*) the outer polar head chains, and (*v*) a possible protein adlayer. The parameters used to model the reflectivity profiles are shown in Table S2 (in the Supporting Information).

3. Results

3.1 Membrane permeabilization by PrP oligomers

Membrane damage was assessed by monitoring the calcein probe release from DOPC/DOPS vesicles. Both the 12-mers and 36-mers of PrP had a leakage effect reaching, respectively, 45% at 500 nM and 50% at 100 nM, whereas the monomeric PrP had no effect with the DOPC/DOPS vesicles within the concentration range of 0-500 nM, as shown in Figure 1. The magnitude of leakage effect is dependent on the concentration of the on- and off-pathway (36- and 12-mers, respectively) oligomers. The on-pathway oligomers caused around 30% leakage of probes to P/L ratio of 1/15000 and 50% leakage to P/L ratio of 1/1500 corresponding to 53

molecules *per* vesicle. The off-pathway oligomers entailed around 15% leakage to P/L ratio of 1/15000 and reached 45% leakage at higher P/L ratio of 1/300. All bound oligomers do not give a disruptive state, and lipid-bound aggregates, which do not lead to efflux, compete with the productive pore-forming state, if any, leading in time to a stop of the efflux. The percentage of leakage increased significantly from 7:3 to 8.5:1.5 molar ratio of DOPS/DOPC for the off-pathway oligomers, whereas it was not significantly changed for the on-pathway oligomers. The fact that the dye leakage does not depend on the PS concentration indicates a different affinity of the on-pathway oligomers compared to the off-pathway ones towards the negative moiety. The higher propensities to disrupt membranes for the on-pathway oligomers than for the off-pathway ones could be explained by an effect of size, since the 36-mers have a mean hydrodynamic diameter of 23 ± 3 nm, measured by DLS, compared to 17.6 ± 1.6 nm for the off-pathway ones. The binding to lipid bilayer of the on-pathway oligomers of higher molecular weight would entail mechanical stress that could stabilize a pore state [44].

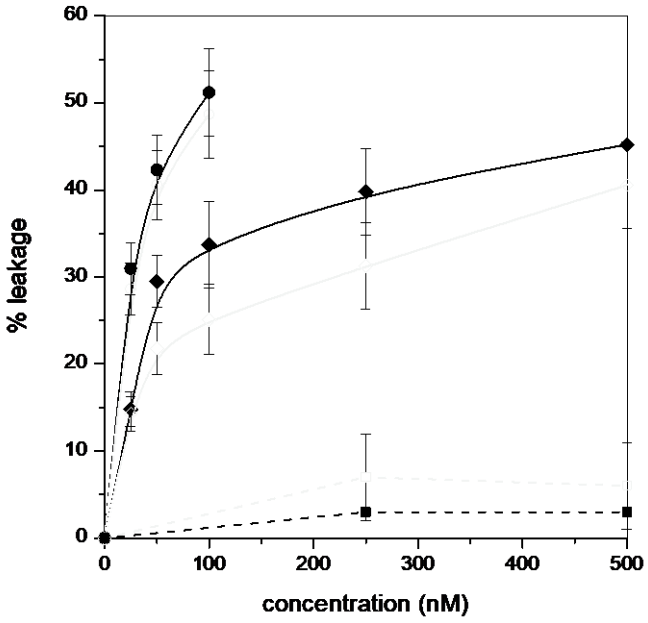

Figure 1. Percentage of calcein leakage of DOPC/DOPS vesicles (0.15 mM) at pH 6.8 induced by the 36-mers of PrP (circles), the 12-mers of PrP (diamonds), and the

corresponding monomers (squares) for a molar ratio of DOPC/DOPS of 7:3 (full symbols) or 8.5:1.5 (open symbols). The lines are guidance for the eye.

3.2 Light-scattering and ThT fluorescence correlation

Kinetics of lipid-induced fibrillation is shown by the addition of monomeric PrP to DOPC/DOPS vesicles suspension, by both ThT binding (Figure 2A) and SLS (Figure 2C). The SLS-ThT binding curves indicated two phenomena: (*i*) the perturbation of the lipid vesicles by PrP binding and (*ii*) the amyloid state of the PrP expressed by the increase in dye binding. The intensity at 633 nm increased instantly after addition of the monomeric PrP, showing the increase in total mass and size of the protein bound-vesicles. It should be noted that the PrP monomer conversion at the vesicle surface is performed at a lipid-to-protein molar ratio of 50/1. In the same conditions, DLS measurements show that vesicle size increases from 110 nm up to 500 nm during PrP monomer binding, whereas the size of lipid suspensions remains significantly unchanged upon addition of the off-pathway oligomers (Figure S3 in the Supporting information).

The intensity measured at 633 nm increased within 1 minute at the addition of oligomers to the DOPC/DOPS vesicles suspensions, showing the rapid and high binding of the off-pathway oligomers to the negatively charged vesicles (Figure 2D). The change in ThT intensity is immediate after addition of the 12-mers to the DOPC/DOPS suspension and remains constant for 1 hour (Figure 2B). The ThT intensity increased from 0.76 to 0.95 in the presence of DOPC/DOPS (Figure 2B), while the pure oligomer at a concentration of 2 µM gave an intensity of 0.805 ± 0.005. These lipid-bound oligomers have higher ThT affinities than the solvated 12-mers, corroborating the lipid-induced conformational change of the 12-mers (Figure 2B). The contact of the oligomers with the lipid bilayer induces the

conformational change of the β-structured 12-mers to an enriched β-state conformers, as supported by the following FTIR-ATR results obtained on SLBs (Figure 3B).

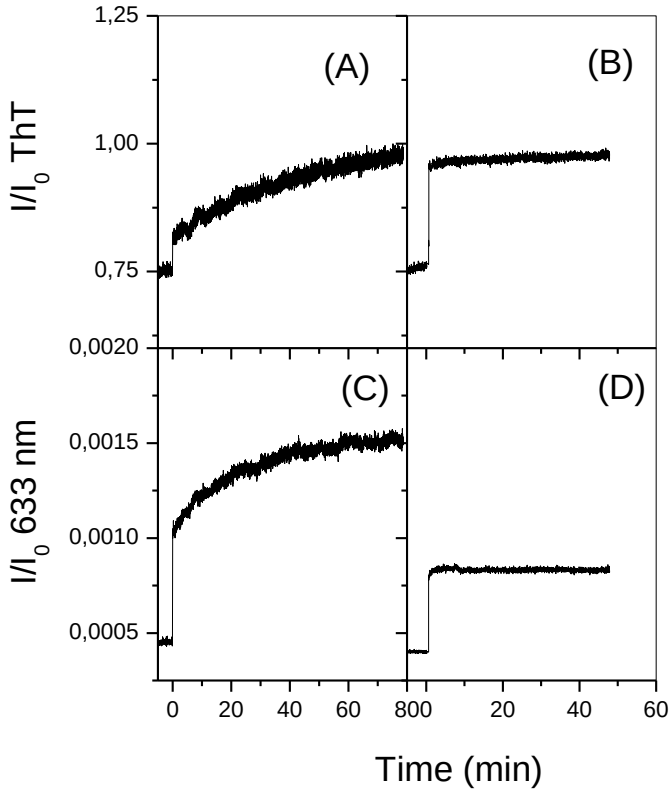

Figure 2. ThT binding (A, B) and SLS (C, D) experiments for PrP 12-mers (B, D), at a concentration of 2 µM, compared to the corresponding experiments for the monomer (A, C), at an equivalent concentration of 5 µM of PrP, in contact with DOPC/DOPS liposomes at lipid concentration of 0.2 mg/mL.

3.3 Conformational changes of PrP oligomer *versus* monomer bound to lipid bilayers

The percentage of Amide I' in each secondary structural elements were determined from FTIR-ATR spectra, recorded as a function of adsorption time of, either PrP monomer, or off-pathway oligomers, on DOPC/DOPS bilayers (Figure 3). From our spectral analysis, PrP monomers in deuterated solution at pD 6.5 contains 40% of α-helix and this content decreases to 34 % at 30 min and to 28 % at 240 min upon contact with membrane (Table S1). The lipid

environment entails for PrP monomers a conformational change from α-helix to β-structure, giving rise to intermolecular β-sheet absorbing at 1630 cm^{-1} and to intermolecular β-sheet at 1614 cm^{-1} (Table S1). We only reported in Figure 3A the content in intermolecular β-sheets at 1614 cm^{-1}, which is an indicator of the amyloid fibrillation [41]. This lipid-induced α-to-β conversion of PrP is in agreement with previously published data [18, 19]. The percentage of Amide I' band component at 1614 cm^{-1} was found to be 3% for the monomeric PrP at time 0 and is indeed likely due to the contribution of Phe and Trp residues. Once the adsorbed amount of PrP reached the plateau value of 6 mg/m^2, the ratio of intermolecular β-sheets in the polypeptide backbone (1614 cm^{-1}) reached 11.5% at 240 min (Figure 3A). The increase in intermolecular β-sheets content for the adsorbed PrP layer gives evidence of the promotion of fibril formation without a lag phase at the lipid interface (Figure 3A). Other studies show an accelerating effect of lipids on the prion fibrillation [18, 19].

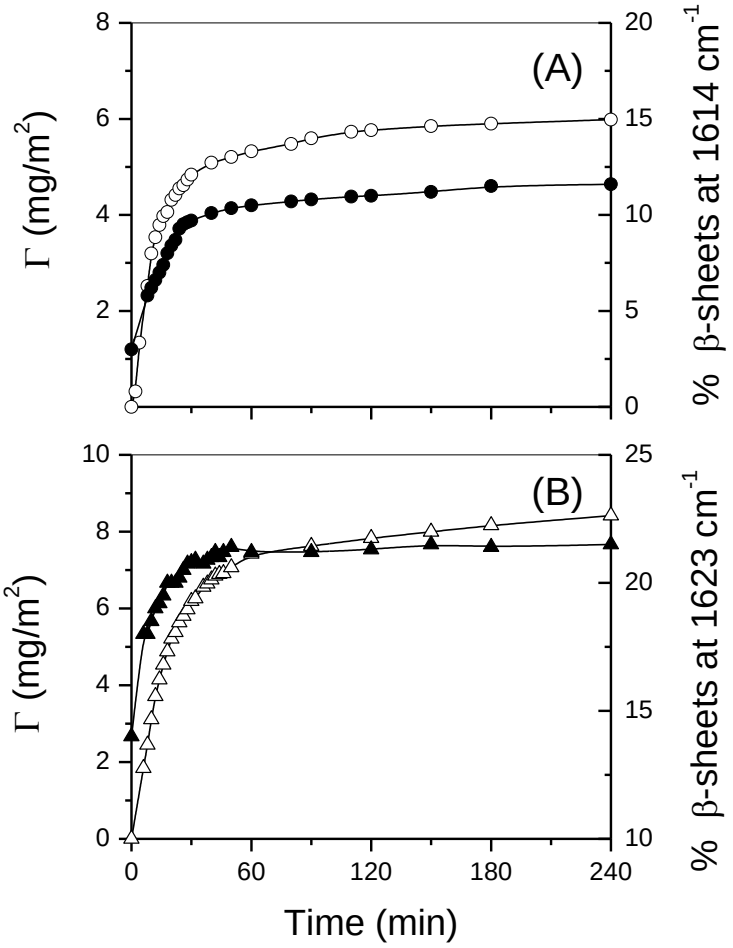

Figure 3. The left axis represents the adsorbed protein amount (open symbols) onto supported DOPC/DOPS bilayer for the monomeric PrP at a bulk concentration of 5 µM (A) and of 12-mer at 5µm equivalent monomer concentration (B). The right axis represents the % of the infrared component band area (full symbols) at 1614 cm^{-1} (A), assigned to intermolecular β-sheets, or at 1623 cm^{-1} (B), attributed to intramolecular β-sheets.

The off-pathway oligomers in solution contain 12% of intermolecular β-sheets, absorbing at 1614 cm^{-1}, and 24% of intramolecular β-sheets, composed of 13% of the polypeptide backbone absorbing at 1623 cm^{-1} and 14% at 1630 cm^{-1} (Table S1). The secondary structures of the off-pathway oligomers are also affected by the lipid bilayer, as shown by the increase of the content in β-sheets (1623 cm^{-1}) to the detriment of the content in β-sheets structure at

1630 cm^{-1} during adsorption (Figure 3B) but no increase in content in intermolecular β-sheets at 1614 cm^{-1} is observed (Table S1). The hydrophobic environment of the lipid membrane generates *de novo* β-structured lipid-bound oligomers, which do not evolve to further amyloid aggregation (Figure 3B). The conformational "snapshot" state of the lipid-induced intermediates corresponding to 30 min of monomer adsorption on SLBs contains 18% of peptide carbonyls involved in intramolecular β-sheets absorbing at 1623 cm^{-1}, 11% of intramolecular β-sheets absorbing at 1630 cm^{-1}, and 9% of peptide carbonyls involved in intermolecular β-sheets absorbing at 1614 cm^{-1}.

3.4 PrP oligomer interaction with SLBs by SNR

3.4.1 Structure of the pure lipid bilayer from SNR

In the absence of protein, the system consisted of a SiO_2 layer above the silicon substrate, the adsorbed lipid bilayer, and aqueous buffer. The naked silicon wafers were fitted without any free parameter (Fresnel calculation). The SiO_2 layer was found to be a single layer of 5.0 ± 0.3 Å thickness with an average roughness of ~1 Å. The bilayer for each sample was fitted, either by a single fit from the D_2O dataset only (not shown), or were co-refined using both D_2O and H_2O datasets, by constraining the thickness and the change in experimental SLD of each contrast to the same values (Figures 4 and 5). In the H_2O contrast, the fringes associated with the bilayer were hardly visible since the SLD of the acyl chains was very close to that of the aqueous buffer (Figures 4B and 5B). By considering these two methods (D_2O only or co-refinement), the model fitting with the four-layer model gave an overall bilayer thickness of 54 ± 3 and 58 ± 2 Å, for the two prepared bilayers, which were subsequently used for the lipid-induced PrP intermediates and the off-pathway oligomers, respectively, in agreement with DOPC/DOPS total lengths. For these two bilayers, the solvent fractions found for the

hydrophobic acyl chain regions were about 85 and 81%, respectively. This corresponds to the surface fraction occupied by the membrane on the silicon surface, in good agreement with data published previously [45]. The hydrophilic heads of the upper layer were solvated at ~60%, giving SLD close to that of the buffer (Figure 4C and 5C). Note that the SLD profiles for the pure lipid bilayer could be slightly different between both contrasts for each PrP species, since the samples are actually different. We performed one experiment *per* contrast, restarting from one lipid deposit on a new silicon wafer, but the two distinct SLBs were nicely reproducible.

The structural parameters of the phospholipid bilayers were then used as references to investigate the conformation and the degree of membrane insertion of the different PrP oligomers during membrane interaction. The resulting model parameters are summarized in Table 1.

A

pure lipid bilayer					**"PrP penetration" hypothesis**					**"solvent penetration" hypothesis**		
layers	***t***	***r***	**exp. SLD**	**solvent**	***t***	***r***	**exp. SLD**	**solvent**	**PrP penetration**	**exp. SLD**	**solvent**	**solvent penetration**
heads in	19	1	3.15	21	23	2	**3.43**	21	**29**	3.15	**28**	**+7**
tails in/out	13	1	1.04	19	16	1	**1.69**	19	**19**	1.04	**29**	**+10**
heads out	20	1	4.60	57	25	2	**5.29**	57	**68**	4.60	**74**	**+17**

B

pure lipid bilayer					**"PrP penetration" hypothesis**					**"solvent penetration" hypothesis**		
layers	***t***	***r***	**exp. SLD**	**solvent**	***t***	***r***	**exp. SLD**	**solvent**	**PrP penetration**	**exp. SLD**	**solvent**	**solvent penetration**
heads in	23	1	2.95	16	20	1	**3.63**	16	**69**	2.95	**33**	**+17**
tails in/out	12	1	0.77	15	17	2	**1.95**	15	**34**	0.77	**33**	**+18**
heads out	25	1	4.97	66	24	1	**4.72**	66	**<0**	4.97	**60**	**-6**
PrP	-	-	-	-	72	2	5.98	88	-	5.98	88	-

Table 1. Physical parameters of the supported lipid bilayer, before (left) and after exposure to (A) lipid-induced on-pathway PrP intermediates or (B) PrP off-pathway oligomers (12-mers). The calculation results presented in the middle part follows the assumption that bilayer

modification comes from PrP recruitment; the right part of the table follows the assumption of additional buffer penetration but without loss of lipids. Significant changes in structural parameters are marked in bold. *t* (Å): layer thickness (± 1 Å); *r* (Å): roughness between one layer and the adjacent previous one (± 1 Å); PrP or solvent penetration: percent of volume fraction (± 2%); exp. SLD (x 10^{-6} $Å^{-2}$): experimental scattering length density (SLD) of the layer (± 0.05 x 10^{-6} $Å^{-2}$); solvent: percent buffer content of the layer (± 2% in volume). The experimental SLD takes into account the solvent content that is noted in the adjacent column. For the theoretical SLD, see Table S2.

3.4.2 The lipid-induced on-pathway intermediates.

After 30 min of exposure to the lipid bilayer, the PrP monomers injected in the subphase were actually β-sheeted intermediates due to the lipid-induced conformational changes, as shown in the FTIR-ATR experiments (Figure 3A). In the presence of the lipid-bound intermediates, the SNR data measured in D_2O showed no deviation of the position of the first oscillation (observed at $q \approx 0.058$ $Å^{-1}$) but only a change in its amplitude (Figure 4A). That means there was no significant modification of the membrane thickness but rather strongly suggests a change in the bilayer composition. The data of PrP in interaction with the bilayer in D_2O and H_2O contrasts have been fitted together using the co-refinement option, by assuming two different hypotheses. The first one is to attribute the experimental SLD change upon PrP assemblies interaction to the penetration of the protein solely and not to the solvent, the second one exclusively to an additional solvent income into the lipid bilayer. The two hypotheses enable to fit correctly the experimental results by a four-layer model (Table 1). Since no fit was possible with a five-layer model, the presence of the protein is excluded at the lipid interface. Moreover, rinsing with pure buffer does not desorb the lipid-induced PrP intermediates, as checked by our FTIR-ATR experiments. Therefore, the second hypothesis

(solvent penetration only) can be ruled out and only the model of insertion of the lipid-bound intermediates into the bilayer can fit the experimental data with a four-layer model. With a protein SLD (in D_2O contrast) at about 3.3 x 10^{-6} $Å^{-2}$, the fit gave a volume fraction of inserted proteins of 19% in the tail region and 68% in the headgroups of the out leaflet (Table 1). Nevertheless, it could also be suggested that the insertion of the PrP assemblies in the lipid bilayer could entail some partial hydration within the headgroups of the external leaflet. The total bilayer thickness increased from 54 ± 3 to 65 ± 2 Å, suggesting that these lipid-bound intermediates penetrated the bilayer without appreciable external protrusion (Figure 4A). In the H_2O contrast, the lipid bilayer was hardly not visible, as mentioned above, but was "revealed" by the protein insertion within the membrane (Figure 4B).

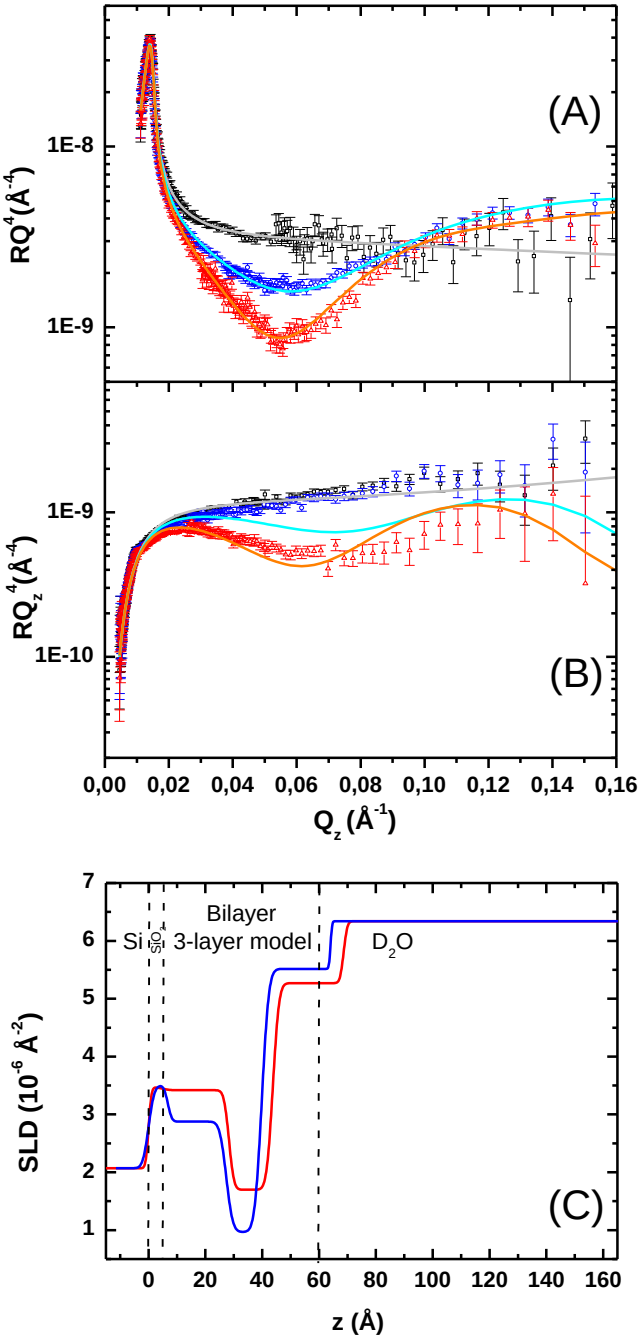

Figure 4. Specular neutron reflectivity profiles of lipid-induced on-pathway PrP intermediates in interaction with a supported lipid membrane. (A, B) SNR profiles in 100% D_2O (A) or 100% H_2O (B) contrast of the naked silicon wafer (black squares), of the pure (in the absence of PrP) supported membrane bilayer made of hydrogenated DOPC/DOPS (7:3) phospholipids in 20 mM MOPS buffer, pD (A) or pH (B) 7.2, (blue circles), and SNR profiles of the same bilayer in the presence of lipid-induced PrP intermediates (red triangles) in the same buffers.

Solid lines (gray, cyan, and orange, for the corresponding data) are the best fits obtained with the four- or five-layer model described in the text. (C) Scattering length density profiles for the pure bilayer (blue curve) or for the membrane in the presence of lipid-induced PrP intermediates (red curve) are shown in the D_2O contrast only but are extracted from the co-refinement reflectivity data analysis from both D_2O and H_2O contrasts.

3.4.3 The off-pathway oligomers.

In the case of the PrP 12-mers (*i.e.* the off-pathway oligomers), the minimum of the SNR spectrum in D_2O was shifted towards the low *q*-values (Figure 5A), meaning that the membrane/PrP oligomers system was thicker than its associated single supported bilayer. In the H_2O contrast, the reflectivity profile was very "soft" and rough (Figure 5B), compared to the spectrum observed for the lipid-bound on-pathway intermediates in the same contrast showing a more marked oscillation (Figure 4B). The reflectivity curves were modeled, using the same co-refinement approach as above, and can be fitted using a five-layer model. An additional protein layer of about 72 ± 1 Å, with a solvent volume fraction of about 88%, was introduced in the multilayer framework to fit the data (Figure 5C, Table 1). Therefore, in contrast to the lipid-induced on-pathway intermediates, the off-pathway oligomers (12-mers) form an additional layer in the vicinity of the outer leaflet membrane. The 88% solvent volume fraction of this layer can be interpreted partly as hydration of the protein but mostly as a partial protein adsorption on the bilayer, such as "patches". We might therefore evaluate at least 12% the surface fraction occupied by the adsorbed protein on the bilayer surface. No significant change in the thickness of the bilayer itself was observed, whereas the SLD profiles of the overall bilayer leaflets were modified (Figure 5C), suggesting that the PrP 12-mer may also reside in the internal region of the membrane. However, in a "PrP penetration" hypothesis, with fixing the water content and taking a protein SLD of 3.3 x 10^{-6} $Å^{-2}$ (D_2O

contrast), the calculation of PrP penetration gave senseless results (negative values of PrP insertion in the outer lipid heads, meaning that some protein should leave from this layer) and invalidate this assumption. So, only the solvent penetration hypothesis was relevant, giving a small amount of supplementary buffer inserted into the bilayer.

Overall, our results showed that the lipid-induced on-pathway species penetrated deeply into the membrane without significant proteic protrusion, whereas the off-pathway species produced along the β-aggregation of PrP monomers in solution formed an adsorbed “patched” layer at the external lipid surface, as illustrated in Scheme 2.

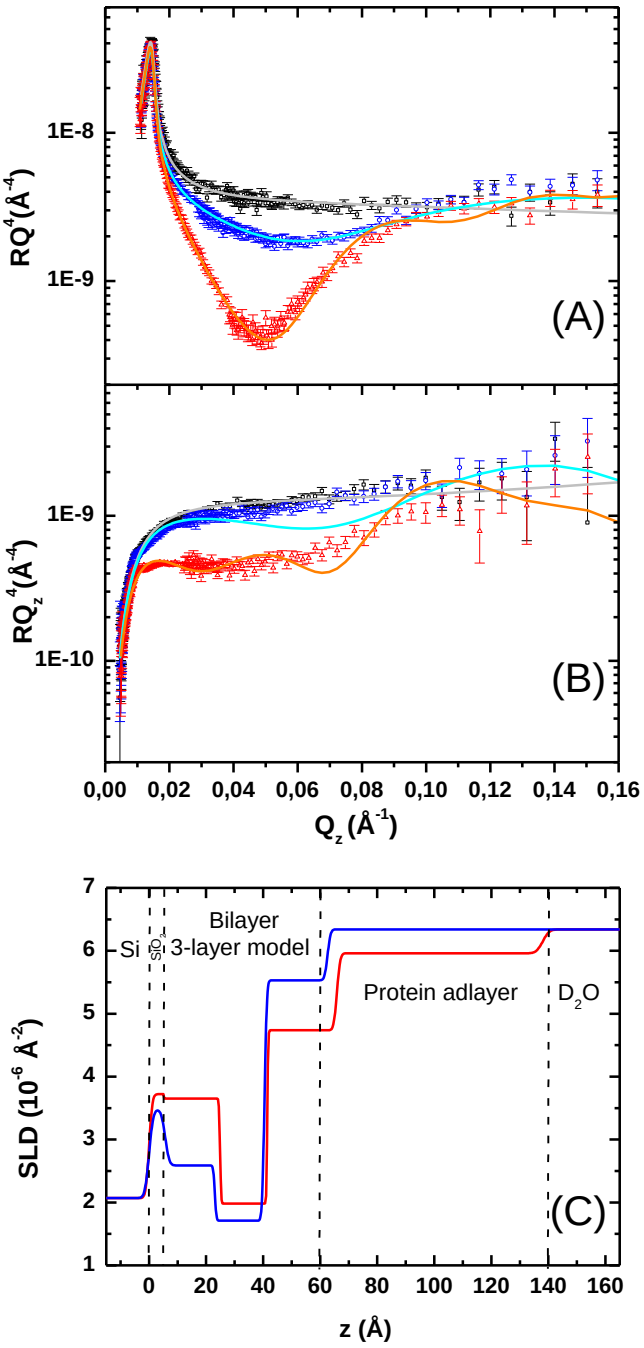

Figure 5. Specular neutron reflectivity profiles of PrP off-pathway oligomers (12-mers) in interaction with a supported lipid membrane. (A, B) SNR profiles in 100% D_2O (A) or 100% H_2O (B) contrast of the naked silicon wafer (black squares), of the pure (in the absence of PrP) supported membrane bilayer made of hydrogenated DOPC/DOPS (7:3) phospholipids in 20 mM MOPS buffer, pD (A) or pH (B) 7.1, (blue circles), and SNR profiles of the same bilayer in the presence of the PrP off-pathway oligomers (red triangles) in the same buffers.

Solid lines (gray, cyan, and orange, for the corresponding data) are the best fits obtained with the four- or five-layer model described in the text. (C) Scattering length density profiles for the pure bilayer (blue curve) or for the membrane in the presence of the PrP off-pathway oligomers (red curve) are shown in the D_2O contrast only but are extracted from the co-refinement reflectivity data analysis from both D_2O and H_2O contrasts.

Scheme 2: (A) membrane-mediated aggregation of the monomeric PrP leading to β-intermediates inserted in lipid bilayers and (B) interaction of off-pathway oligomers at lipid interface.

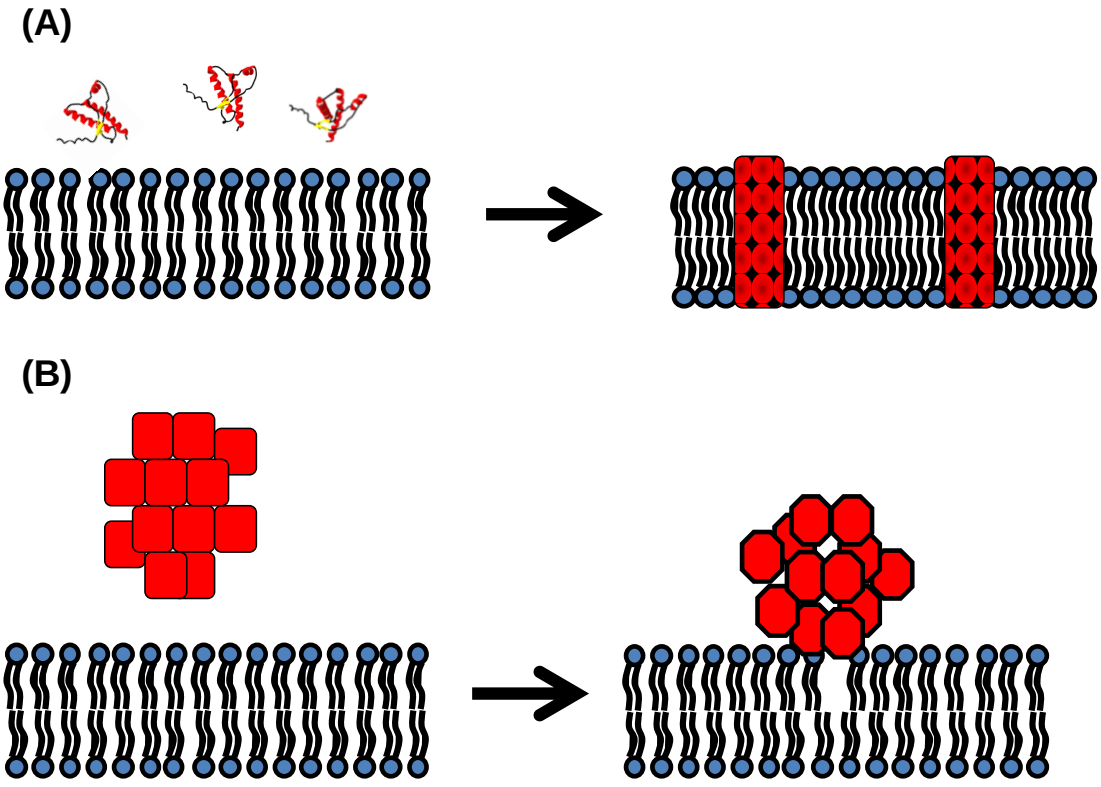

4. Discussion and Conclusion

We present in this paper a range of biophysical experiments aiming at elucidating the membrane interaction of purified off-pathway PrP oligomers to lipid-induced PrP

intermediates. First, we focused our experimental work on the membrane permeabilization by off-pathway PrP oligomers produced in solution to decipher the mechanism of amyloidogenecity and toxicity. The off-pathway oligomers are species produced *in vitro* along PrP fibrillation but do not give rise to the formation of the fibrillar end products [25]. Previous studies have shown that oligomeric PrP species are toxic towards cells [46]. These entities are β-structured in solution and contains 14% of the polypeptide backbone in intramolecular β-sheets at 1623 cm^{-1}, suggesting β-sheeted structures involving, either a larger number of strands, or a more planar conformation [41]. Besides, flatness of the β-sheet has been proposed to be critical for high-affinity ThT binding [47]. The measured ThT affinity for the free off-pathway oligomers in solution (Figure 3B) is also in agreement with the presence of such structural β-arrangement.

Results from calcein-dye leakage show that PrP oligomers could permeabilize negatively charged lipid vesicles in a rapid all-or-none fashion regarding the unchanged vesicles distribution by DLS (Figure S3). In the literature, many hypotheses could explain the permeabilization of lipid bilayers by oligomeric species. It has been suggested for other amyloidogenic proteins that membrane permeabilization by oligomeric species occurs through the formation of pore-like complexes inserted in the lipid membrane [23, 48, 49]. The conformational change observed for the off-pathway oligomers is entailed by the presence of lipids to a rearranged β-structure by decreasing the parallel β-sheets content at 1630 cm^{-1} to a higher content in more planar β-sheets (1623 cm^{-1}) (Figure 3B). This increase in 1623 cm^{-1} is also correlated to the ThT increased affinity observed for the lipid-bound oligomers in Figure 2B. This lipid-induced conformational change of the PrP oligomers would be in favor of the pore hypothesis [18, 44, 50]. Although the pore formation accounts for membrane disruption, some facets remain unexplained if we consider the size of the spherical soluble oligomers reaching 17 nm diameter for the 12-mers up to 23 nm diameter for the 36-mers with reference

to the measured hydrodynamic diameter. It has been reported that vesicles containing high amounts of negatively charged moieties are ruptured more easily by mechanical forces [51]. However, we show that not solely 12-mers are membrane active but also soluble on-pathway oligomers of higher molecular weight in a concentration range where the freshly dissolved PrP monomer is inefficient (Figure 1). If the binding mode to the lipid bilayers is indeed of prime importance, it is obvious that soluble oligomers contain structural features, enabling the destabilization of the lipid membrane.

It should be also noticed that the binding of the off-pathway PrP oligomers on SLBs do not cause lipid release as observed by our ATR experiments. A detergent-like mechanism causing membrane disruption by the accumulation of large oligomeric species can then be excluded for the PrP oligomers, in contrast with that have been reported for the action of oligomeric species from Aβ or IAPP peptides [48, 52].

From our SNR experiments, the off-pathway oligomers, presenting lytic activities, do not insert into the lipid bilayer. This experimental observation in addition to those of an enriched β-structure of the lipid-bound oligomers enable to conclude that the binding of the large PrP assemblies destabilize the outer leaflet of the membrane, allowing water molecules to penetrate inside the lipid bilayer and causing dye leakage. Our observations from dye-leakage assays made up at lipid-to-protein ratio of 300/1 are consistent with the existence of an initially membrane-disruptive state upon binding of the off-pathway oligomers to the bilayer, that could reorganizes into a state much less disruptive rather than a model of pore-forming species.

In the literature, another hypothesis could explain the permeabilization of lipid bilayers by oligomeric species, linked to their ability to form amyloid fibers onto the surface of lipid vesicles [53]. For example, the damage of DOPC:DOPS vesicles by IAPP oligomers were caused by the mechanical disruption of the lipid membrane as a result of the associated

growth of amyloid-like fibrils [54]. From our ThT-SLS and FTIR-ATR experiments, we could observe that the ThT positive lipid-bound state of the off-pathway oligomers is related to the presence of planar β-sheets rather than to intermolecular β-sheets found in amyloid aggregates. Besides, the SNR results show the formation of a protein adlayer on the external lipid membrane, less compatible with further fibril elongation known to lead more hydrophobic entities.

Unlike the off-pathway oligomers, the lipid-induced PrP intermediates from the monomer conversion in lipid environment is inserted in the lipid bilayer. Moreover the lipid-induced species present a completely different secondary structure that of the off-pathway oligomers, with a higher content in intermolecular β-sheets, showing its multimeric state. The intermolecular β-sheets, known to be also present in amyloid aggregates, have a high affinity to the ThT fluorescent probe [28]. And we show that these early PrP intermediates are also ThT positive aggregates by our SLS-ThT experiments (Figure 2). The study at the early stage of formation of these lipid-induced intermediates ensures to characterize the oligomeric states rather than fibrillar end-products [55]. The high interfacial concentration in PrP species obtained during monomer adsorption on SLBs is in favor of the formation of β-sheeted oligomeric intermediates resulting from the α-helix unfolding in the hydrophobic environment. The mode of interaction of these oligomeric species with lipid membrane is different from that of the off-pathway oligomers. The insertion of the lipid-induced PrP intermediates as shown by SNR is corroborated by the increase in vesicles size upon monomer conversion, as shown by DLS at similar lipid to protein ratio used for SLS-ThT experiments (Figure S3).

Thanks to the SNR and ATR experiments performed at identical conditions, we can propose two distinct mechanisms of interaction with PrP intermediates generated along the fibrillation in solution or on the accelerated fibrillation at lipid interface. The former operates as a

surface-acting agent more than a pore-forming species, whereas the latter inserts in the lipid bilayer, both of them having a putative role in neurotoxicity. Our conclusions coincide with emerging ideas concerning the production of different oligomeric species potentially neurotoxic, whether the β-aggregation or the fibrillation starts from the amyloidogenic proteins free in solution or is embedded in lipids [56]. However, the formation of these PrP intermediates occur at high molar concentration ratio of lipid to protein reaching, in our case, around 6:1 for ATR and 50:1 for SLS-ThT experiments. The high lipid-to-protein molar ratio needed for the formation of the lipid-induced PrP intermediates raises the question of *in vivo* relevance of lipid membrane as non-specific catalyst of the protein fibrillation. At the present time, the question of the localization in the cell of PrP misfolding is still under debate [57]. If a high interfacial concentration in PrP monomers localized at a specific composition of the cell membrane is reached, it is then possible, due to the high conformational flexibility of the prion protein, to generate β-enriched intermediates behaving in a strongly different manner than lytic soluble oligomer

Author information

Corresponding Author: Dr. Sylvie Noinville, Laboratoire MONARIS, UMR 8233, Sorbonne Université, CNRS, 4 place Jussieu, F-75005 Paris, France; Telephone: (33) 144 273 289; Fax: (33) 144 273 021; E-mail: sylvie.noinville@sorbonne-universite.fr

Abbreviations

PrP, prion protein; DOPC, 1,2-dioleoyl-sn-glycero-3-phosphocholine; DOPS, 1,2-dioleoyl-sn-glycero-3-phospho-L-serine; SLB, supported lipid bilayer; ThT, thioflavin T; FTIR-ATR, Fourier transform infrared spectroscopy-attenuated total reflection; SNR, specular neutron reflectometry; SLS, static light scattering; DLS: dynamic light scattering.

Acknowledgements

This work was funded by INRA, CNRS and the Laboratoire Léon-Brillouin (Neutron source facility, CEA, France).

REFERENCES

[1] S.B. Prusiner, Novel proteinaceous infectious particles cause scrapie, Science 216 (1982) 136-44. https://doi.org/ 10.1126/science.6801762

[2] A.R. Walmsley, F. Zeng and N.M. Hooper, Membrane topology influences N-glycosylation of the prion protein, EMBO J. 20 (2001) 703-12. https://doi.org/10.1093/emboj/20.4.703

[3] G.S. Baron, K. Wehrly, D.W. Dorward, B. Chesebro and B. Caughey, Conversion of raft associated prion protein to the protease-resistant state requires insertion of PrP-res (PrP(Sc)) into contiguous membranes, EMBO J. 21 (2002) 1031-40.

[4] C. Bate and A. Williams, Monoacylated Cellular Prion Protein Modifies Cell Membranes, Inhibits Cell Signaling, and Reduces Prion Formation, J. Biol. Chem. 286 (2011) 8752-8758. https://doi.org/10.1074/jbc.M110.186833

[5] J. Ma, The role of cofactors in prion propagation and infectivity, PLoS Pathog 8 (2012) e1002589. https://doi.org/10.1371/journal.ppat.1002589

[6] J. Collinge and A.R. Clarke, A general model of prion strains and their pathogenicity, Science 318 (2007) 930-6. https://doi.org/10.1126/science.1138718

[7] M.K. Sandberg, H. Al-Doujaily, B. Sharps, A.R. Clarke and J. Collinge, Prion propagation and toxicity in vivo occur in two distinct mechanistic phases, Nature 470 (2011) 540-542. https://doi.org/10.1038/nature09768

[8] E. Ferreiro, C.R. Oliveira and C.M.F. Pereira, The release of calcium from the endoplasmic reticulum induced by amyloid-beta and prion peptides activates the mitochondrial apoptotic pathway, Neurobiology of Disease 30 (2008) 331-342. https://doi.org/10.1016/j.nbd.2008.02.003

[9] B.L. Kagan, R. Azimov and R. Azimova, Amyloid peptide channels, J. Membr. Biol. 202 (2004) 1-10. https://doi.org/10.1007/s00232-004-0709-4

[10] I.H. Solomon, E. Biasini and D.A. Harris, Ion channels induced by the prion protein: Mediators of neurotoxicity, Prion 6 (2012) 40-45.https://doi.org/10.4161/pri.6.1.18627

[11] G.P. Gorbenko and P.K.J. Kinnunen, The role of lipid-protein interactions in amyloid-type protein fibril formation, Chem. Phys. Lipids. 141 (2006) 72-82. https://doi.org/10.1016/j.chemphyslip.2006.02.006

[12] A. Rawat, R. Langen and J. Varkey, Membranes as modulators of amyloid protein misfolding and target of toxicity, Biochim. Biophys. Acta, Biomembr. 1860 (2018) 1863-1575. https://doi.org/10.1016/j.bbamem.2018.04.011

[13] S. Noinville, J.F. Chich and H. Rezaei, Misfolding of the prion protein: linking biophysical and biological approaches, Vet. Res. 39 (2008) 48. https://doi.org/10.1051/vetres:2008025

[14] P. Critchley, J. Kazlauskaite, R. Eason and T.J. Pinheiro, Binding of prion proteins to lipid membranes, Biochem. Biophys. Res. Commun. 313 (2004) 559-67. https://doi.org/10.1016/j.bbrc.2003.12.004
[15] J. Kazlauskaite, N. Sanghera, I. Sylvester, C. Venien-Bryan and T.J. Pinheiro, Structural changes of the prion protein in lipid membranes leading to aggregation and fibrillization, Biochemistry 42 (2003) 3295-304. https://doi.org/10.1021/bi026872q
[16] T. Luhrs, R. Zahn and K. Wuthrich, Amyloid Formation by Recombinant Full-length Prion Proteins in Phospholipid Bicelle Solutions, J. Mol. Biol. 357 (2006) 833-841. https://doi.org/10.1016/j.jmb.2006.01.016
[17] J. Kazlauskaite, A. Young, C.E. Gardner, J.V. Macpherson, C. Venien-Bryan and T.J. Pinheiro, An unusual soluble beta-turn-rich conformation of prion is involved in fibril formation and toxic to neuronal cells, Biochem. Biophys. Res. Commun. 328 (2005) 292-305. https://doi.org/10.1016/j.bbrc.2004.12.172
[18] J.F. Chich, C. Chapuis, C. Henry, J. Vidic, H. Rezaei and S. Noinville, Vesicle permeabilization by purified soluble oligomers of prion protein: a comparative study of the interaction of oligomers and monomers with lipid membranes, J. Mol. Biol. 397 (2010) 1017-30. https://doi.org/10.1016/j.jmb.2010.02.013
[19] N. Sanghera, M.J. Swann, G. Ronan and T.J. Pinheiro, Insight into early events in the aggregation of the prion protein on lipid membranes, Biochim. Biophys. Acta 1788 (2009) 2245-51. https://doi.org/10.1016/j.bbamem.2009.08.005
[20] F. Wang, X. Wang, C.-G. Yuan and J. Ma, Generating a Prion with Bacterially Expressed Recombinant Prion Protein, Science 327 (2010) 1132-1135. https://doi.org/10.1126/science.1183748
[21] F. Wang, S. Yin, X. Wang, L. Zha, M.-S. Sy and J. Ma, Role of the Highly Conserved Middle Region of Prion Protein (PrP) in PrP-Lipid Interaction, Biochemistry 49 (2010) 8169-8176. https://doi.org/10.1021/bi101146v
[22] M. Bhattacharya and P. Dogra, Self-Assembly of Ovalbumin Amyloid Pores: Effects on Membrane Permeabilization, Dipole Potential, and Bilayer Fluidity, Langmuir 31 (2015) 8911-8922. https://doi.org/10.1021/acs.langmuir.5b02074
[23] H.A. Lashuel and P.T. Lansbury, Jr., Are amyloid diseases caused by protein aggregates that mimic bacterial pore-forming toxins?, Q. Rev. Biophys. 39 (2006) 167-201. https://doi.org/10.1017/S0033583506004422
[24] M. Fandrich, Oligomeric Intermediates in Amyloid Formation: Structure Determination and Mechanisms of Toxicity, J. Mol. Biol. 421 (2012) 427-440. https://doi.org/10.1016/j.jmb.2012.01.006
[25] F. Eghiaian, T. Daubenfeld, Y. Quenet, M. van Audenhaege, A.P. Bouin, G. van der Rest, J. Grosclaude and H. Rezaei, Diversity in prion protein oligomerization pathways results from domain expansion as revealed by hydrogen/deuterium exchange and disulfide linkage, Proc. Natl. Acad. Sci. U.S.A. 104 (2007) 7414-9. https://doi.org/10.1073/pnas.0607745104
[26] M. Adrover, K. Pauwels, S. Prigent, C. de Chiara, Z. Xu, C.l. Chapuis, A. Pastore and H. Rezaei, Prion Fibrillization Is Mediated by a Native Structural Element That Comprises Helices H2 and H3, J. Biol. Chem. 285 (2010) 21004-21012. https://doi.org/10.1074/jbc.M110.111815
[27] H. Rezaei, F. Eghiaian, J. Perez, B. Doublet, Y. Choiset, T. Haertle and J. Grosclaude, Sequential Generation of Two Structurally Distinct Ovine Prion Protein Soluble Oligomers Displaying Different Biochemical Reactivities, J. Mol. Biol. 347 (2005) 665-679. https://doi.org/10.1016/j.jmb.2005.01.043

[28] M.R.H. Krebs, E.H.C. Bromley and A.M. Donald, The binding of thioflavin-T to amyloid fibrils: localisation and implications, J. Struct. Biol. 149 (2005) 30-37. https://doi.org/10.1016/j.jsb.2004.08.002
[29] R. Richter, A. Mukhopadhyay and A. Brisson, Pathways of Lipid Vesicle Deposition on Solid Surfaces: A Combined QCM-D and AFM Study, Biophys. J. 85 (2003) 3035-3047. https://doi.org/10.1016/S0006-3495(03)74722-5
[30] S.A. Bellingham, B.B. Guo, B.M. Coleman and A.F. Hill, Exosomes: vehicles for the transfer of toxic proteins associated with neurodegenerative diseases?, Frontiers in physiology 3 (2012) e124. https://doi.org/10.3389/fphys.2012.00124
[31] N. Brouette, G. Fragneto, F. Cousin, M. Moulin, M. Haertlein and M. Sferrazza, A neutron reflection study of adsorbed deuterated myoglobin layers on hydrophobic surfaces, J. Coll. Interf. Sci. 390 (2013) 114-120. https://doi.org/10.1016/j.jcis.2012.09.040
[32] A. Chenal, L. Prongidi-Fix, A.l. Perier, C. Aisenbrey, G.g. Vernier, S. Lambotte, G. Fragneto, B. Bechinger, D. Gillet, V. Forge and M. Ferrand, Deciphering Membrane Insertion of the Diphtheria Toxin T Domain by Specular Neutron Reflectometry and Solid-State NMR Spectroscopy, J. Mol. Biol. 391 (2009) 872-883. https://doi.org/10.1016/j.jmb.2009.06.061
[33] Anton P. Le Brun, Cathryn L. Haigh, Simon C. Drew, M. James, Martin P. Boland and Steven J. Collins, Neutron Reflectometry Studies Define Prion Protein N-terminal Peptide Membrane Binding, Biophys. J. 107 (2014) 2313-2324. https://doi.org/10.1016/j.bpj.2014.09.027
[34] A. Martel, L. Antony, Y. Gerelli, L. Porcar, A. Fluitt, K. Hoffmann, I. Kiesel, M. Vivaudou, G. Fragneto and J.J. de Pablo, Membrane Permeation versus Amyloidogenicity: A Multitechnique Study of Islet Amyloid Polypeptide Interaction with Model Membranes, J. Am. Chem. Soc. 139 (2016) 137-148. https://doi.org/10.1021/jacs.6b06985
[35] A. Junghans, E.B. Watkins, J. Majewski, A. Miranker and I. Stroe, Influence of the Human and Rat Islet Amyloid Polypeptides on Structure of Phospholipid Bilayers: Neutron Reflectometry and Fluorescence Microscopy Studies, Langmuir 32 (2016) 4382-4391. https://doi.org/10.1021/acs.langmuir.6b00825
[36] H. Rezaei, D. Marc, Y. Choiset, M. Takahashi, G. Hui Bon Hoa, T. Haertle, J. Grosclaude and P. Debey, High yield purification and physico-chemical properties of full-length recombinant allelic variants of sheep prion protein linked to scrapie susceptibility, Eur. J. Biochem. 267 (2000) 2833-9. https://doi.org/10.1046/j.1432-1033.2000.01347.x
[37] S. Noinville, M. Revault, M.-H. Baron, A. Tiss, S. Yapoudjian, M. Ivanova and R. Verger, Conformational changes and orientation of Humicola lanuginosa lipase on a solid hydrophobic surface: an in situ interface FTIR-ATR study, Biophys. J. 82 (2002) 2709-2719. https://doi.org/10.1016/S0006-3495(02)75612-9
[38] M. Revault, H. Quiquampoix, M.H. Baron and S. Noinville, Fate of prions in soil: trapped conformation of full-length ovine prion protein induced by adsorption on clays, Biochim. Biophys. Acta 1724 (2005) 367-74. https://doi.org/10.1016/j.bbagen.2005.05.005
[39] F. Sokolowski and D. Naumann, FTIR study on thermal denaturation and aggregation of recombinant hamster prion protein SHaPrP90-232, Vib. Spectrosc 38 (2005) 39-44. https://doi.org/10.1016/j.vibspec.2005.02.005
[40] S. Krimm and J. Bandekar, Vibrational spectroscopy and conformation of peptides, polypeptides, and proteins, Adv. Protein Chem. 38 (1986) 181-364. https://doi.org/10.1016/S0065-3233(08)60528-8

[41] G. Zandomeneghi, M.R. Krebs, M.G. McCammon and M. Fandrich, FTIR reveals structural differences between native beta-sheet proteins and amyloid fibrils, Protein Sci. 13 (2004) 3314-21. https://doi.org/10.1110/ps.041024904
[42] F. Cousin, F. Ott, F. Gibert and A. Menelle, EROS II: A boosted time-of-flight reflectometer for multi-purposes applications at the Laboratoire Leon Brillouin, Eur. Phys. J. Plus 126 (2011) 109. https://doi.org/10.1140/epjp/i2011-11109-6
[43] A. Nelson, Co-refinement of Multiple-contrast neutron/X-ray Reflectivity Data Using MOTOFIT, J. Appl. Crystallogr 39 (2006) 273-276. https://doi.org/10.1107/S0021889806005073
[44] H.W. Huang, F.Y. Chen and M.T. Lee, Molecular mechanism of peptide-induced pores in membranes, Phys. Rev. Lett. 92 (2004) 198304. https://doi.org/10.1103/PhysRevLett.92.198304
[45] G. Fragneto, T. Charitat, F. Graner, K. Mecke, L. Perino-Gallice and E. Bellet-Amalric, A fluid floating bilayer, Europhys. Lett. 53 (2001) 100-106. https://doi.org/10.1209/epl/i2001-00129-8
[46] S. Simoneau, H. Rezaei, N. Sales, G. Kaiser-Schulz, M. Lefebvre-Roque, C. Vidal, J.G. Fournier, J. Comte, F. Wopfner, J. Grosclaude, H. Schatzl and C.I. Lasmezas, In vitro and in vivo neurotoxicity of prion protein oligomers, PLoS Pathog. 3 (2007) 1175-1186. https://doi.org/10.1371/journal.ppat.0030125
[47] M. Biancalana, K. Makabe, A. Koide and S. Koide, Molecular mechanism of thioflavin-T binding to the surface of beta-rich peptide self-assemblies, J. Mol. Biol. 385 (2009) 1052-63. 10.1016/j.jmb.2008.11.006
[48] Michele F. Sciacca, Samuel A. Kotler, Jeffrey R. Brender, J. Chen, D.-k. Lee and A. Ramamoorthy, Two-Step Mechanism of Membrane Disruption by A-beta through Membrane Fragmentation and Pore Formation, Biophys. J. 103 (2012) 702-710. https://doi.org/10.1016/j.bpj.2012.06.045
[49] M.J. Volles and P.T. Lansbury, Zeroing in on the Pathogenic Form of alpha-Synuclein and Its Mechanism of Neurotoxicity in Parkinson's Disease, Biochemistry 42 (2003) 7871-7878. https://doi.org/10.1021/bi030086j
[50] S.M. Butterfield and H.A. Lashuel, Amyloidogenic Protein-Membrane Interactions: Mechanistic Insight from Model Systems, Angew. Chem. Int. Ed. 49 (2010) 5628-5654. https://doi.org/10.1002/anie.200906670
[51] S.D. Shoemaker and T.K. Vanderlick, Intramembrane electrostatic interactions destabilize lipid vesicles, Biophys. J. 83 (2002) 2007-14. https://doi.org/10.1016/S0006-3495(02)73962-3
[52] T.L. Williams, B.R.G. Johnson, B. Urbanc, A.T.A. Jenkins, S.D.A. Connell and L.C. Serpell, Ab42 oligomers, but not fibrils, simultaneously bind to and cause damage to ganglioside-containing lipid membranes, Biochem. J. 439 (2011) 67-77. https://doi.org/10.1042/BJ20110750.
[53] R. Friedman, R. Pellarin and A. Caflisch, Amyloid Aggregation on Lipid Bilayers and Its Impact on Membrane Permeability, J. Mol. Biol. 387 (2009) 407-415. https://doi.org/10.1016/j.jmb.2008.12.036
[54] M.F.M. Engel, L. Khemtemourian, C.C. Kleijer, H.J.D. Meeldijk, J. Jacobs, A.J. Verkleij, B. de Kruijff, J.A. Killian and J.W.M. Hoppener, Membrane damage by human islet amyloid polypeptide through fibril growth at the membrane, Proc. Natl. Acad. Sci. U.S.A. 105 (2008) 6033-6038. https://doi.org/10.1073/pnas.0708354105
[55] J.T. Jarrett and P.T. Lansbury, Jr., Seeding "one-dimensional crystallization" of amyloid: a pathogenic mechanism in Alzheimer's disease and scrapie?, Cell 73 (1993) 1055-8. https://doi.org/10.1016/0092-8674(93)90635-4

[56] V. Rondelli, P. Brocca, S. Motta, M. Messa, L. Colombo, M. Salmona, G. Fragneto, L. Cantu and E. Del Favero, Amyloid-beta Peptides in interaction with raft-mime model membranes: a neutron reflectivity insight, Sci. Rep. 6 (2016) 20997. https://doi.org/10.1038/srep20997

[57] A. Fehlinger, H. Wolf, A. Hossinger, Y. Duernberger, C. Pleschka, K. Riemschoss, S. Liu, R. Bester, L. Paulsen, S.A. Priola, M.H. Groschup, H.M. Schätzl and I.M. Vorberg, Prion strains depend on different endocytic routes for productive infection, Sci. Rep. 7 (2017) 6923. https://doi.org/10.1038/s41598-017-07260-2

Supporting Information

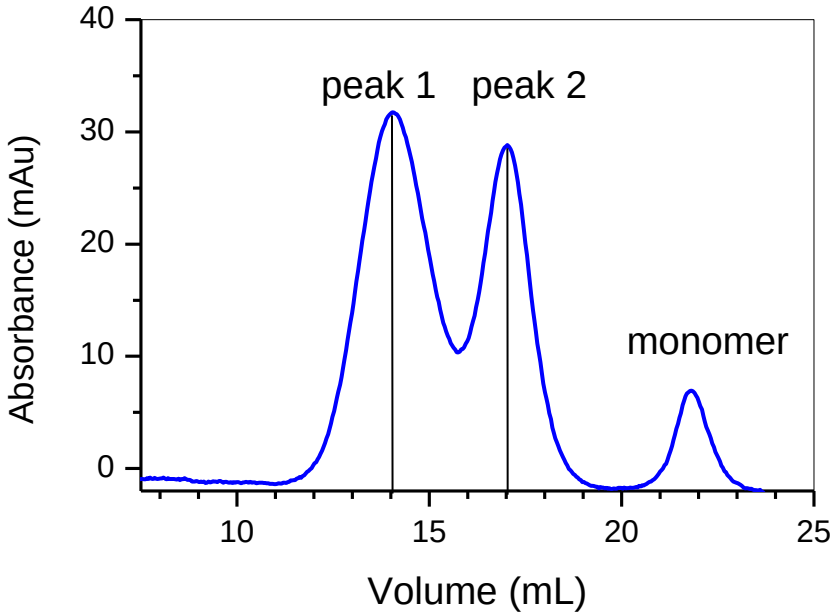

Figure S1. Size-exclusion chromatogram obtained after 8 min incubation of monomeric PrP at 80 µM in citrate buffer at 50°C to produce on-pathway (peak 1) and off-pathway (peak 2) oligomers.

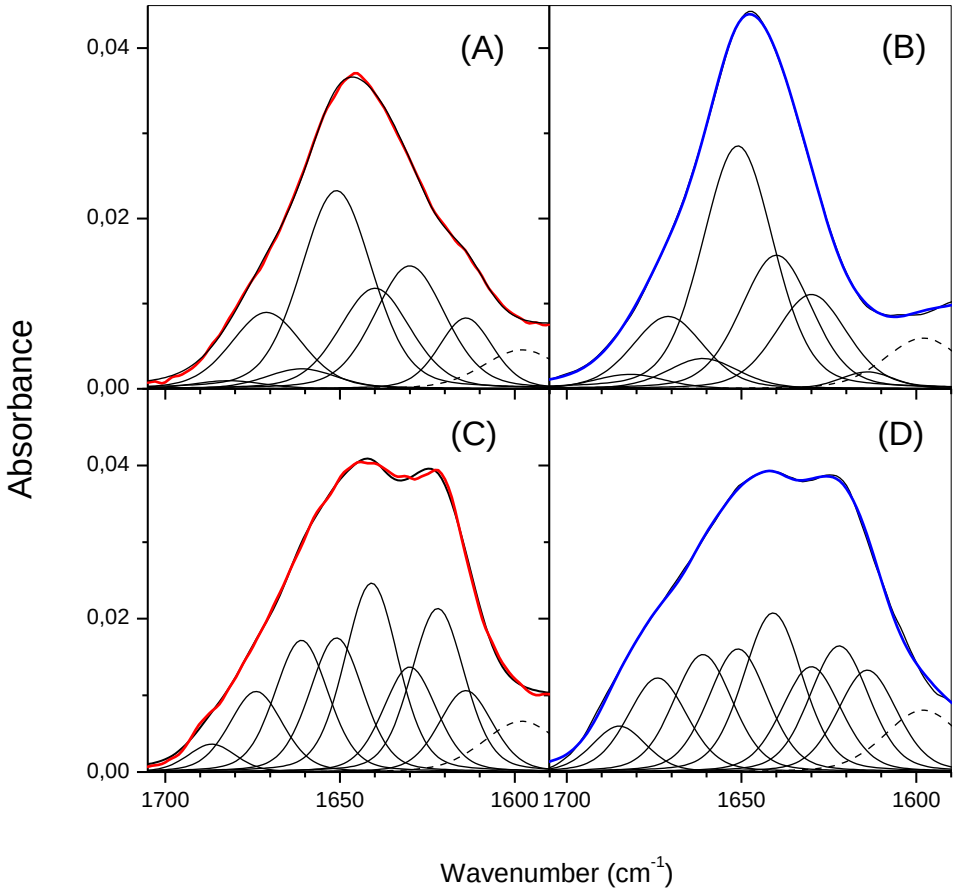

Figure S2. ATR- corrected spectra after 30 minutes of contact with lipid bilayer (red curves) and transmission spectra (blue curves) in deuterated buffer at pD 6.8 (A) of monomeric PrP after 30 min incubation with lipid bilayer (B) of monomeric PrP at 180 µM in solution, (C) of off-pathway oligomeric PrP after 30 min incubation with lipid bilayer, (D) of off-pathway oligomeric PrP at 40 µM in solution. The dashed line corresponds to the ν(CO) of the Asp and Glu residues.

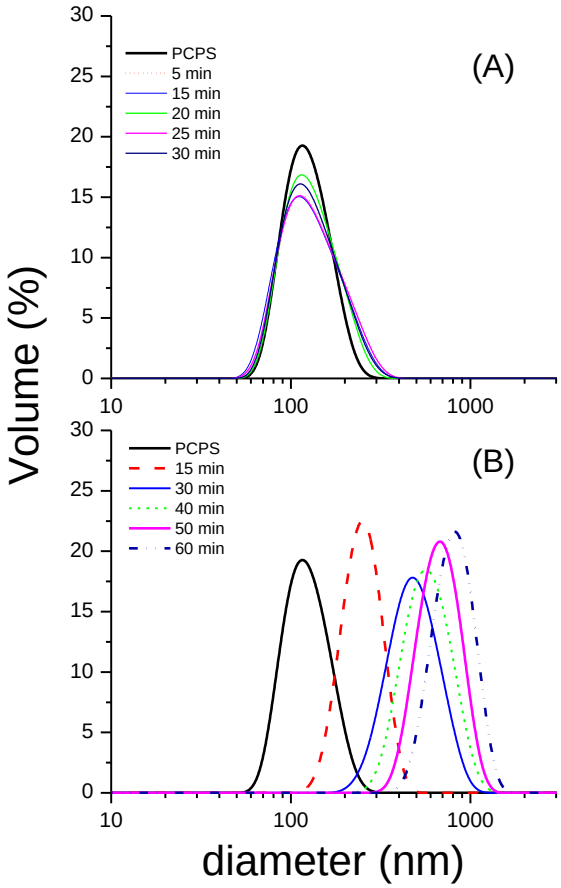

Figure S3. DLS measurements of PCPS vesicles free (bold line) or in addition of off-pathway oligomers at a equivalent monomer concentration of 500 nM and for a lipid-to-protein molar ratio of 300/1 (A) or of PrP monomer at 500 nM and for a lipid-to-protein molar ratio of 62/1 (B) at different times of interaction.

Supplemental Table 1: Assignment of Amide I' component bands and spectral decomposition analysis of the monomeric PrP and oligomeric PrP in deuterated MOPS buffer at pD 7 (T=0min) and after exposure of 30 min or 240 min to the lipid bilayer. % Amide I' is expressed by the ratio of area of each component band to the total area of the Amide I'.

PrP monomer	%Amide I'			Assignment
	T= 0 min	T=30 min	T= 240 min	
1614 - 1630	3 16	9 21	11.5 23	Intermolecular β-sheet – β-sheet
1640	20	17	18	Hydrated random
1650	36	34	28	Random or α-helices
1661	11	4	5	Random or α-helices
1671	10	13	12.5	Random or β-turn
1682	3	2	2	Random or β-turn
PrP oligomer	%Amide I'			Assignment
	T= 0 min	T=30 min	T= 240 min	
1614	12	9	8	Intermolecular β-sheet
1623	13	18	21	β-sheet
1630	14	11	5	β-sheet
1640	18	21	27	Hydrated random
1651	14	14.5	11	Random or α-helices
1661	14	14.5	15	Random or β-turn
1674	10	9	10	Random or β-turn
1685	5	3	3	Random or β-turn

Supplemental Table 2: Molecular scattering length densities (SLD) used in SNR calculations.

Compound	SLD (x 10^{-6} $Å^{-2}$)
Si	2.07
SiO_2	3.47
DOPC:DOPS (7:3) heads	2.3 (in D_2O) or 2.01 (in H_2O)
DOPC:DOPS (7:3) tails	-0.21
prion	3.30 (in D_2O) or 1.88 (in H_2O)
solvent	6.34 (D_2O) or -0.56 (H_2O)

Conflict of interest

The authors declare no conflict of interest.

Author contributions :

SC conducted and analyzed SNR experiments, and had a part in shading the paper, FC performed SNR experiments and contributed to data analyses, HR contributed to protein production and conceived ThT-SLS experiments, SN conducted and performed biophysical experiments, analyzed data, and wrote the paper.